Acta Materialia 111 (2016) 85–95

Contents lists available at ScienceDirect

Acta Materialia

journal homepage: www.elsevier.com/locate/actamat

Full length article

Effects of trace elements (Y and Ca) on the eutectic Ge in Al–Ge based alloys

J.H. Li [a, *], N. Wanderka [b], Z. Balogh [c], P. Stender [c], H. Kropf [b], M. Albu [d], Y. Tsunekawa [e], F. Hofer [d], G. Schmitz [c], P. Schumacher [a, f]

[a] Institute of Casting Research, Montanuniversität Leoben, Austria
[b] Helmholtz-Zentrum Berlin für Materialien und Energie GmbH, Hahn-Meitner-Platz 1, 14109 Berlin, Germany
[c] Institut für Materialwissenschaft, Universität Stuttgart, Heisenbergstraße 3, D-70569 Stuttgart, Germany
[d] Institute for Electron Microscopy and Nanoanalysis, Graz University of Technology, Graz Center for Electron Microscopy, Austria
[e] Toyota Technological Institute, Hisakata 2-12-1, Tempaku, Nagoya 468-8511, Japan
[f] Austrian Foundry Research Institute, Leoben, Austria

ARTICLE INFO

Article history:
Received 1 February 2016
Received in revised form
11 March 2016
Accepted 14 March 2016

Keywords:
Al–Ge alloy
Segregation
Solute entrainment
Eutectic solidification
HAADF-STEM
Atom probe tomography

ABSTRACT

Effects of trace elements (0.2Y and 0.2Ca (wt%) on the eutectic Ge in high purity Al–20Ge (wt%) alloys were investigated by multi-scale microstructure characterization techniques. Particularly, the distribution of trace elements (Y and Ca) within the eutectic Ge and/or at the interface between eutectic Ge and eutectic Al was investigated by atomic resolution high angle annular dark field scanning transmission electron microscopy (HAADF-STEM) imaging and atom probe tomography (APT). The combined investigations indicate Al–Y and Al–Ca co-segregations. Such co-segregations change significant morphology and growth of the eutectic Ge. In addition, large Al_2Ge_2Y and Al_2Ge_2Ca phases were also measured. The modification of eutectic Ge is discussed in terms of previously postulated modification mechanisms: twin plane re-entrant edge growth mechanism, impurity-induced twinning, and growth restriction of eutectic Ge.

1. Introduction

Trace elements may have a dominant effect on the microstructure evolution of Al based eutectic systems. For example, a trace addition of e.g. 200 ppm Sr in Al–Si alloys can modify the eutectic Si from plate-like to fibrous morphology and thereby greatly improve the mechanical properties [1]. Possible modification mechanisms of eutectic Si have been postulated [2–6]. It is generally accepted that impurity induced twinning (IIT) [3] and twin plane re-entrant edge (TPRE) growth mechanism [4,5], as well as poisoning of the TPRE [6] are effective under certain conditions. Among these mechanisms, the modifier agents (e.g. Sr) only within eutectic Si were assumed to be responsible for the modification of eutectic Si. However, the distribution of the modifier agents within eutectic Si has been observed to be inhomogeneous by using atomic resolution high angle annular dark field scanning transmission electron microscopy (HAADF-STEM) imaging and atom probe tomography (APT) [7–10]. It has been clearly demonstrated that the modification of eutectic Si is related to the formation of the multiple Si twins with a high density [7,8] and/or the co-segregations of the modifiers together with eutectic Si and eutectic Al [9,10]. By contrast, in the case of eutectic Ge, it is not clear yet whether IIT, TPRE and poisoning of the TPRE mechanisms are still valid, although the TPRE mechanism was originally observed in the pure Ge [3–5]. Furthermore, effects of trace elements (e.g. Y and Ca) on the formation of co-segregations and thereby the growth of eutectic Ge also still remain to be explored.

Similar to the Al–Si alloy system, Al–Ge also represents a simple eutectic system, although the eutectic point and temperature of binary Al–Ge alloys (53 wt% at 424 °C) is different from that of binary Al–Si (12.7 wt% at 577 °C) [1]. Apart from these similarities, at least three differences should be highlighted. Firstly, compared to Si, Ge forms growth twins more easily and therefore a preferred <100> texture was not often observed. Instead, Ge grows with a <110> preferred orientation [1]. Secondly, it has been reported that

* Corresponding author. Institute of Casting Research, Montanuniversität Leoben, A-8700 Leoben, Austria.
E-mail address: jie-hua.li@hotmail.com (J.H. Li).

http://dx.doi.org/10.1016/j.actamat.2016.03.043
1359-6454/

Na can modify eutectic Si in Al–Si alloy [2] and eutectic Ge in Al–Ge alloy as well. However, the modification effect and Ge twinning induced by Na is much less pronounced and decrease progressively with the Ge content in Al–Ge alloys [11]. Furthermore, the strong modifier (e.g. Sr) for eutectic Si cannot modify the eutectic Ge [11]. Thirdly, as illustrated in Refs. [4,5], the presence of two or more twinning events provides re-entrant grooves on at least two crystal faces which can act as preferential sites for molecular attachment and thereby favours the growth of the crystal in three dimensions. In the case of eutectic Si, the presence of modifiers at the twin re-entrant edges (for poisoning of the TPRE) has been experimentally supported. However, the distribution of other trace elements (e.g. Y and Ca) at the twin re-entrant edges was not investigated yet, in particular at an atomic scale. Furthermore, the distribution of trace elements at the interface between eutectic Ge and eutectic Al has been also proposed to affect the growth of eutectic Ge [1]. However, such type of investigations is still missing.

In this paper, the microstructure of eutectic Ge in high purity Al–20 wt% Ge alloys with the additions of 0.2 wt% Y and 0.2 wt% Ca was investigated by multi-scale microstructure characterization techniques, including scanning electron microscopy (SEM), HAADF-STEM and APT. In particular, the distribution of trace elements (Y and Ca) within the eutectic Ge and at the interface between eutectic Ge and eutectic Al was investigated using HAADF-STEM and APT, with the aim to elucidate the growth mechanism that controls the microstructure evolution of eutectic Ge.

2. Experimental

A series of Al–20 wt% Ge alloys (wt%, used through the paper in case not specified otherwise) with the additions of 0.2Y and 0.2Ca were prepared using arc melting. The cooling rate was evaluated to be about 200 °C/min. It is noteworthy that Ge was added by Ge (99.998). Y was added by an Al–4Y master alloy manufactured from (99.998) Al and (99.8) Y. Ca was added by an Al–20Ca master alloy produced from (99.998) Al and (99.8) Ca.

The specimens for SEM investigation were mechanically ground using standard metallographic procedures and finally polished with a colloidal silica suspension. For the microstructure characterization, a Zeiss 1540 EsB CrossBeam® workstation was employed. The imaging was performed with a low acceleration voltage of 5 kV using a secondary electron (SE) detector. The use of the low acceleration voltage enables to obtain high resolution images [12].

The samples for TEM investigation were mechanically ground, polished and dimpled to about 30 μm in thickness, and then ion-beam milled using a Gatan Precision Ion Polishing System (PIPS, Gatan model 691). A constant preparation temperature (about −10 °C) was maintained by using a cold stage during ion beam polishing. High resolution TEM was performed using an image-side Cs-corrected JEOL-2100F microscope operated at 200 kV. Atomic scale HAADF-STEM imaging and EDX investigations were performed using a monochromated and probe-corrected FEI Titan3TM G2 60–300 (S/TEM) microscope operated at 300 kV with an X-FEG high-brightness emission gun. The high-resolution images in STEM mode were recorded with a beam diameter of 0.1 nm and a current of 0.04 nA using the HAADF and dark field (DF) detectors. X-ray spectra were acquired by the SuperX detection system (Chemi-STEM™ technology) with a 120 mm acquisition area which reduces significantly the acquisition times. Elemental quantification of the EDX spectra was performed using the K-factor method [13]. The images and spectra were recorded by a Gatan Digiscan unit and Digital Micrograph software, and were corrected for dark current and gain variations.

The needle-like samples of a radius less than 50 nm for APT analysis have been prepared by site-specific FIB milling in the Zeiss 1540 EsB CrossBeam® workstation. The FIB preparation method comprises many steps: (i) cutting the lamella of the eutectic including the area of interest with the interface between eutectic Al and eutectic Ge; (ii) welding the lamella to the micromanipulator; (iii) attaching the lamella to support pillars (pre-sharpened Mo tip) and welding it; (iv) cutting a portion of the tip (one lamella can be prepared into about five tips); (v) ion etching to achieve a desired shape of 50 nm apex radius, and (vi) finally cleaning up to remove Ga implantation with a low kV mode (2 kV). APT measurements were carried out in a local electrode APT instrument build at the University of Münster (now University of Stuttgart), Germany [14]. Field evaporation of atoms from the apex were performed by femtosecond UV laser pulses of 343 nm wavelength with a repetition rate of 200 kHz and a pulse energy of 60 nJ. APT analyses were performed at a tip temperature of 45 K in an ultra-high vacuum (10^{-8} Pa).

3. Results

3.1. SEM

Fig. 1 shows typical microstructures of Al–20Ge alloys without and with the additions of 0.2Y and 0.2Ca, respectively. The microstructure consists of primary aluminium, eutectic Ge and eutectic Al as well as Al_2Ge_2X type (X: Ca, Y) intermetallic phases. All these phases show different contrasts when imaged with the SE detector. The eutectic Ge can be distinguished by its bright contrast. The intermetallic phases can be identified not only by their light grey contrast but also by their morphology, which is rod-like in two dimensions. Finally eutectic Al as well as the primary Al phase is imaged by dark grey contrast.

In the Al–20Ge alloy, eutectic Ge was observed as coarse bright lamellas and fibres, as shown in Fig. 1a and b. In the Al–20Ge–0.2Y alloy, a much finer eutectic Ge structure was observed when compared with the binary Al–20Ge alloy. A deeper insight in the eutectic Ge structure shows an interconnected network of eutectic Ge, as shown in Fig. 1c and d. Similarly, in the Al–20Ge–0.2Ca alloy, a much finer eutectic Ge structure was observed, as shown in Fig. 1e and f. However, in contrast to the Al–20Ge–0.2Y alloy, some spherical eutectic Ge particles were observed in the Al–20Ge–0.2Ca alloy. In addition, intermetallic Al_2Ge_2Y and Al_2Ge_2Ca phases were also observed, as marked by arrows in Fig. 1d and e. These intermetallic phases are similar to the Al_2Si_2Sr phase existing in Al–Si based alloys [8,9].

3.2. TEM

To obtain structural and compositional properties of the eutectic Ge, different imaging TEM techniques were combined. Fig. 2 shows a bright field (BF) TEM image as well as a high resolution TEM (HRTEM) micrograph of a eutectic Ge particle in Al–20Ge alloy. Several parallel arranged {111} twin traces in Fig. 2b were observed in the eutectic Ge phase of a sample aligned with [011] zone axis parallel to the electron beam. Twin traces are marked by a white solid arrow. Accurate crystallographic information about the planar defects of twins and stacking faults can be revealed by electron diffraction [15]. Fig. 2c shows the corresponding selected area electron diffraction (SAED) pattern of Ge from Fig. 2b. This SAED pattern is typical of a diamond crystal in [011] zone axis orientation containing {111} planar defects of twins. The additional spots located at one third between the main diffraction spots along <111> directions represent the presence of {111} twins. This presence of twins along the Ge plates confirms the TPRE growth mechanism of eutectic Ge reported in Refs. [5,6].

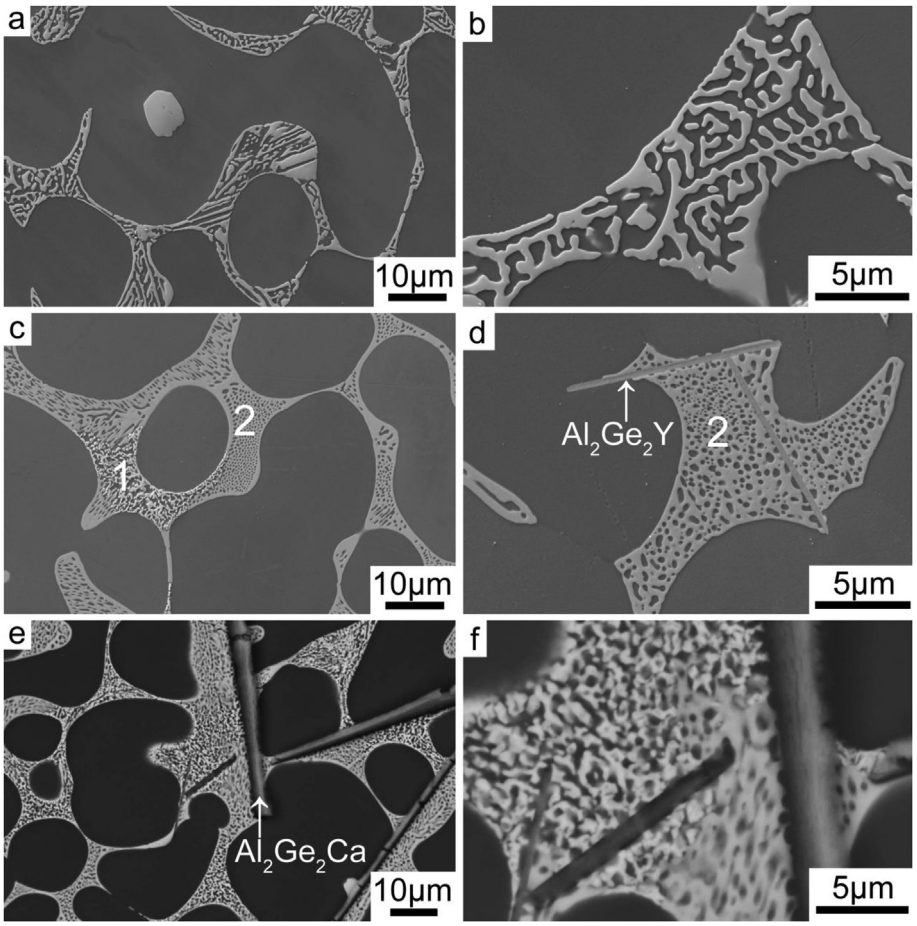

Fig. 1. Eutectic structures observed by SEM in Al–20Ge alloy (a, b), Al–20Ge–0.2Y alloy (c, d) and Al–20Ge–0.2Ca alloy (e, f), respectively.

The eutectic Ge phase in the alloy with 0.2 Y additions is shown in Fig. 3 using BF TEM and HRTEM as well. Apart from the parallel {111} twins in eutectic Ge marked by a white solid arrow in Fig. 3b and c, the second possible {111} co-zonal twin system with an angle of 70.5° to the parallel aligned twins is also visible (marked in Fig. 3b). The comparison of the microstructure of the eutectic Ge with Y- (Fig. 3) and without Y additions (Fig. 2) indicates that there are no significant changes of the eutectic Ge phase when observed in two dimensions in BF TEM images. The investigation of eutectic Ge in the Al–20Ge–0.2Y alloy using BF STEM and HAADF STEM as illustrated in Fig. 4 does not show any segregations of Y in the eutectic Ge. However, an energy-dispersive X-ray spectroscopy (EDX) line scan in STEM along the solid line in Fig. 4b indicates segregation of Y of about 5 at% along the twins. Thus, it provides clear evidence of Y segregation. In addition to this Y segregation a high amount of Al > 20 at% was also measured indicating co-segregation of the minority elements. The absence of contrast from Y in the STEM image can be attributed to their similar atom numbers between Y (39) and Ge (32) and the low Y concentration. The enrichment of Y along the twins in eutectic Ge is believed to promote the twin plane re-entrant edge growth mechanism.

Investigations using HAADF STEM were carried out on eutectic Ge in the Al–20Ge–0.2Ca alloy as well. Fig. 5a shows bright eutectic Ge phases surrounded by eutectic Al in a darker contrast. Segregations of Ca could not be observed here. However, the EDX line scan across the eutectic Al–Ge interface (marked in Fig. 5a) as shown in Fig. 5b indicates a Ca enrichment at the interface. A Ca-rich particle of composition $Al_{59.7}Ge_{32}Ca_{8.3}$ (at%) was also measured at the Al–Ge interface. Further examples of eutectic Ge surrounded by eutectic Al are shown in Fig. 6 obtained by HAADF STEM at different magnifications. A Ca-rich particle with a composition Al_2Ge_2Ca at the boundary of the eutectic Ge could be measured as shown in Fig. 6c. However, in contrast to the Al–20Ge–0.2Y alloy, in the Al–20Ge–0.2Ca alloy, no twins were observed in the eutectic Ge, as shown in Figs. 5 and 6, indicating that there is no effect of Ca on Ge twinning. The formation of $Al_{59.7}Ge_{32}Ca_{8.3}$ and Al_2Ge_2Ca phases in the vicinity of the eutectic Ge indicates that Ca may diffuse out during the growth of eutectic Ge and segregates at the interface between eutectic Ge and eutectic Al.

Given the fact that there is no visible contrast of Y and Ca in HAADF STEM imaging and energy-dispersive X-ray spectroscopy and/or electron energy loss spectroscopy have very strict requirements on the TEM sample thickness and cleanness, it is still very challenging to measure the distribution of Y and Ca within the eutectic Ge or eutectic Al. Therefore APT was applied to clarify details about the element distribution.

3.3. APT

For the Al–20Ge alloy, Fig. 7a shows a reconstruction of 3D elemental map of Al (pink dots) atom positions. The major part of measured volume is eutectic Ge. The investigated volume is $68 \times 67 \times 79$ nm^3. Only 20% of all measured Al atoms are shown in Fig. 7a. For clarity, Ge atoms are omitted. The amount of Al in eutectic Ge is measured to be 5.43 ± 0.01 at% which exceeds the

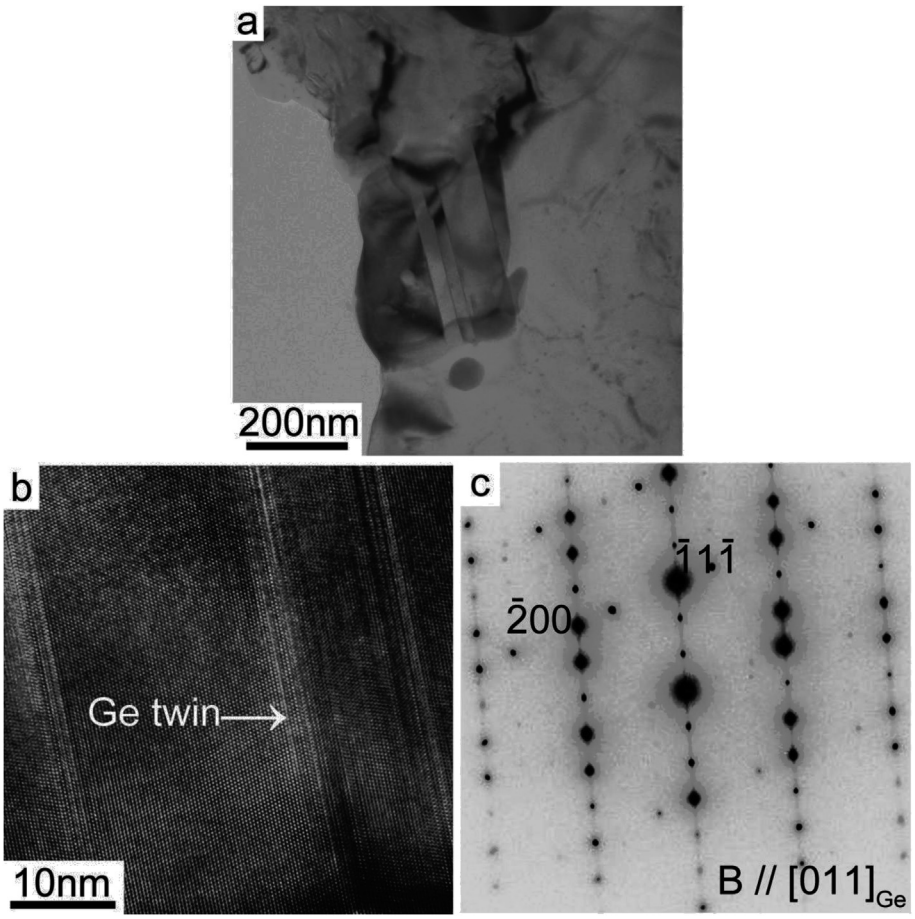

Fig. 2. (a) TEM bright field and (b) high resolution TEM image of the eutectic Ge phase in Al–20Ge alloy observed in $[011]_{Ge}$ zone axis orientation. Parallel {111} Ge twin traces were observed, as marked with a white solid arrow in (b). Corresponding selected area diffraction pattern is presented in (c).

equilibrium solubility limit significantly. We do not believe that this elevated content of Al is due to an obvious artefact of the atom probe method, since the evaporation threshold for Al is significantly less than that for Ge and so only Al loss rather than enrichment can be expected by preferential evaporation. For an accurate analysis regarding a heterogeneous distribution of Al in the eutectic Ge, a sub-volume of 20 × 20 × 10 nm^3 (marked in Fig. 7a) was evaluated in detail. A concentration cluster search module developed by the APT group in Rouen [16] has been applied to the APT data with a threshold $C_{Al} \geq 10$ at%. A 3D visualization of the Al-rich clusters is shown in Fig. 7b. The presented volume contains 23 Al-rich clusters of nearly spherical morphology and an average radius of about 1 nm. Inside the clusters Ge atoms are also shown, but the surrounding single Al and Ge atoms in the sub-volume are not presented for clarity. It is found that nanosized Al-rich clusters consist of 14.14 ± 3.84 at% Al in average. Apart from Al, small amounts of O (0.02 ± 0.01 at%) were also measured, which can be attributed to the impurities during alloy preparation even by arc melting. No other significant impurities were measured, indicating that the arc-melted samples are of a very high purity level.

For the Al–20Ge–0.2Y alloy, Fig. 8a shows a 3D reconstruction of 15% of all measured Al (pink dots), 10% of all measured Y (blue dots) and only 1% of Ge atom positions within the eutectic Ge phase. The investigated volume was 74 × 74 × 160 nm^3. The distribution of Y within the eutectic Ge is found to be inhomogeneous. An area, about 10 nm wide and enriched in Y, is emphasised by an iso-concentration surface (blue colour) at a threshold of 4 at% Y. The compositional correlation between Al, Ge and Y across the Y-rich area is shown in the concentration depth profiles in Fig. 8b determined along a cylinder of 2 nm radius, as marked in Fig. 8a. While the concentration of Ge and Al within the iso-concentration surface is approximately the same (Al = 42.09 ± 2.05 at%, Ge = 48.88 ± 2.01 at%), the amount of Y is much less (Y = 5.10 ± 2.62 at%). Surprisingly, a high amount of Oxygen (O = 4.13 ± 2.64 at%) within the Y-rich area was measured. The given error bar is defined as the 2σ deviation which was used for all APT measurements. According to the measured composition of this region, the Y-rich particle corresponds to a $Al_{42}Ge_{49}Y_5O_4$ phase, which is not consistent with the known equilibrium intermetallic phases (e.g. Al_2Ge_2Y or AlGeY) [17]. Presumably $Ge_{49}Al_{42}Y_5O_4$ is a metastable phase which finally transforms into the stable Al_2Ge_2Y intermetallic phase that is observed by SEM in Fig. 1d.

Fig. 9a shows another example of an APT measurement of a region with a eutectic Al–Ge interface in the Al–20Ge–0.2Y alloy. Both eutectic phases, Al (pink) highlighted by an iso-concentration surface with a threshold of 75 at% Al and Ge (cyan) highlighted by iso-concentration surface with a threshold of 90 at% Ge are shown in an investigated volume of 75 × 74 × 154 nm^3. The corresponding composition depth profile along a cylinder with a radius of 1.5 nm located perpendicular to the eutectic Al–Ge interface is shown in Fig. 9b. It is found that most Y is located within the eutectic Al, while no significant Y is found within eutectic Ge. However, a slight increase of Y content is measured at the interface between eutectic Al and eutectic Ge (see Fig. 9b). A Y-rich particle was also observed

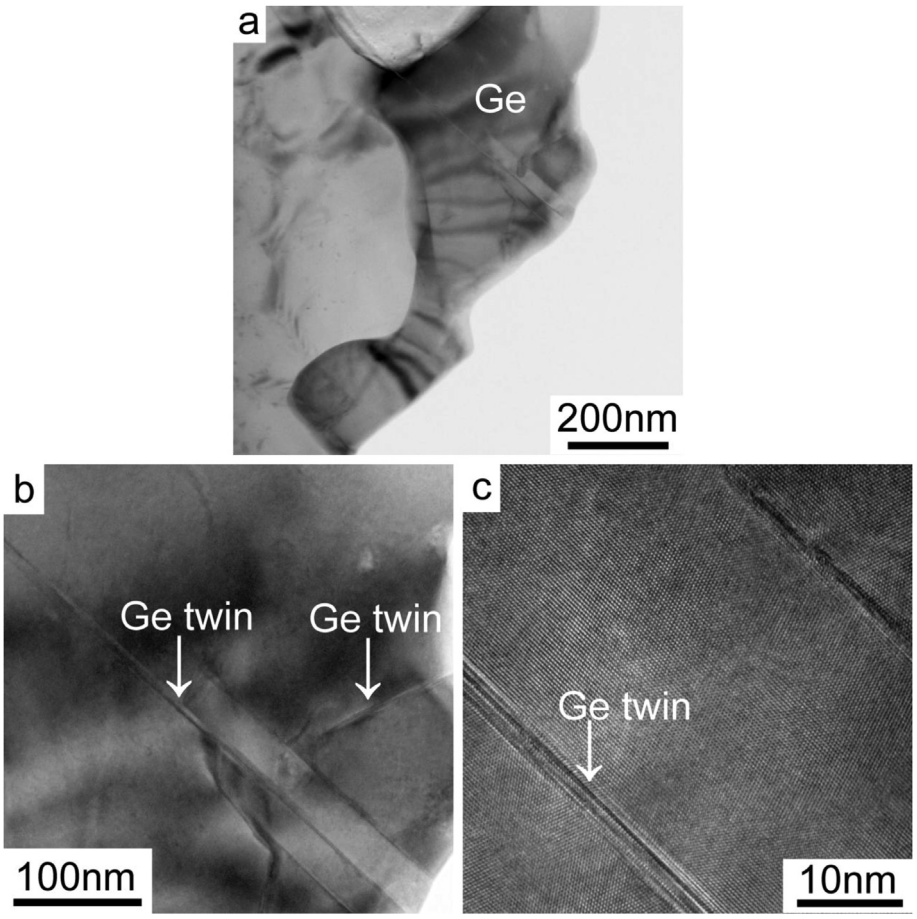

Fig. 3. (a) TEM bright field and (b, c) high resolution TEM images of the eutectic Ge particle in Al–20Ge–0.2Y alloy in $[011]_{Ge}$ zone axis orientation. Parallel Ge twins were observed, as marked by a white solid arrow in (c). The second possible co-axial twin system (with an angle of 70.5°) was also observed, as marked by a white solid arrow in (b).

in the investigated volume, as marked by the blue arrow in Fig. 9a and emphasised by an iso-concentration surface at a threshold of 20 at% Y. The Y-enriched particle contains Al (69.31 ± 1.83 at%), Ge (8.76 ± 2.78 at%) and Y (21.93 ± 2.52 at%). This Y-rich particle can be assigned as $(AlGe)_{3.5}Y_1$ type, assuming that Ge is partially substituted by Al. So the composition is close to the Al_3Y phase which is a stable equilibrium phase in the binary Al–Y diagram.

For the Al–20Ge–0.2Ca alloy, Fig. 10a shows a 3D reconstruction of an APT analysis of the interface between eutectic Al and eutectic Ge. The investigated volume is 65 × 64 × 138 nm^3. Iso-concentration surfaces representing the eutectic Ge are visualized by a threshold of 85 at% Ge. Iso-concentration surfaces of Ca are visualized by a threshold of 8 at%. For clarity, eutectic Al is not shown here. Fig. 10b shows the composition depth profiles along a cylinder with a radius of 4 nm oriented perpendicularly to the interface between eutectic Al and eutectic Ge. Two interfaces were observed, but only one of them shows a significant segregation of Ca. The segregation zone contains Al (40.96 ± 1.40 at%), Ge (36.80 ± 1.45 at%), Ca (15.90 ± 1.67 at%), and O (6.34 ± 1.77 at%). It should be noted that such type of Ca segregation is not rare. It is very often observed at the interfaces between eutectic Al and eutectic Ge even though with fluctuating compositions. Another Ca-rich segregation zone (~6 nm) at the interface between eutectic Al and eutectic Ge (not shown here) contains for example Al (29.93 ± 2.36 at%), Ge (56.48 ± 1.87 at%), Ca (7.52 ± 2.72 at%), and O (6.07 ± 2.74 at%).

Fig. 11a shows a 3D reconstruction of the Al–20Ge–0.2Ca alloy. For clarity only 5% of the Al, 2% of the Ge and 50% of the measured Ca atoms are plotted. The presented volume is 70 × 69 × 79 nm^3, which is only a part of the entire measurement involving ~1 × 10^8 ions. Fig. 11c shows the compositional correlation between Al, Ge and Ca in the composition depth profiles along the cylinder, marked in Fig. 11a. In the volume extending from 0 to ~25 nm depth, the distribution of Ca within the eutectic Ge is quite heterogeneous. The cluster-search module [16] was used to analyse local Ca enrichments. Small Ca-enriched particles are highlighted in Fig. 11b. The chemical composition of the particles has to be estimated from a very small volume (the average number of detected atoms per Ca-rich particle is ~120) with a radius of about 1 nm. But on average, the particles contain Al (33.70 ± 1.49 at%), Ge (38.84 ± 1.54 at%), Ca (26.63 ± 1.40 at%), and O (0.82 ± 0.29 at%). This composition is very close to the composition of the Al_2Ge_2Ca phase. In the Ge rich volume from 25 to ~50 nm depth, the distribution of Ca appears to be homogeneous. No Ca-enriched clusters are detected. The volume from ~50 nm to ~65 nm is Al-rich.

Fig. 12a shows another 3D reconstruction obtained from the eutectic Ge. For clarity, the Ge atoms were omitted, only 50% of the Ca atoms and 10% of the Al atoms are shown. The investigated volume amounts to 73 × 75 × 142 nm^3. Significant Ca-enriched clusters were observed within the eutectic Ge. Two Ca-rich particles were displayed by an iso-concentration surface at a threshold of 2.5 at% Ca. Fig. 12b shows one single Ca-rich particle embedded in eutectic Ge, enlarged from Fig. 12a (the displayed volume is 63 × 71 × 37 nm^3). The composition depth profile along the shown

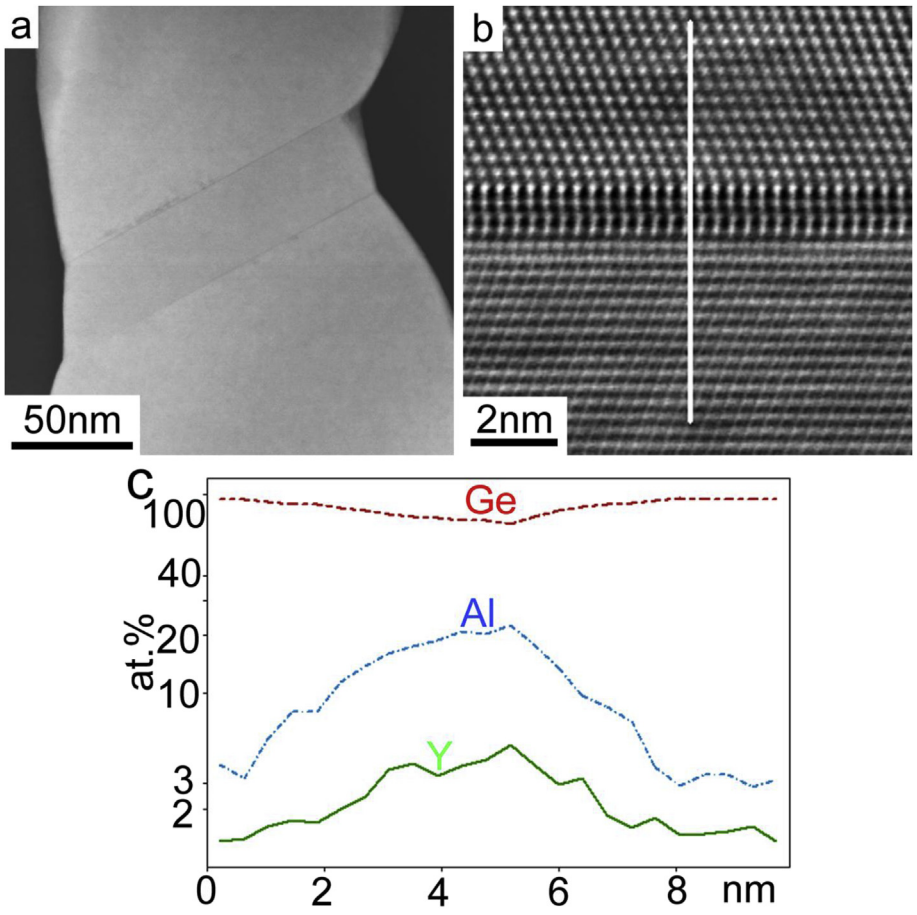

Fig. 4. (a, b) HAADF STEM images and (c) EDX line scan of the Ge particle in Al–20Ge–0.2Y alloy imaged in $[011]_{Ge}$ zone axis orientation. Parallel {111} Ge twin traces were observed, as shown in (a, b). A significant Y enrichment was measured along the Ge twin, as shown in (c).

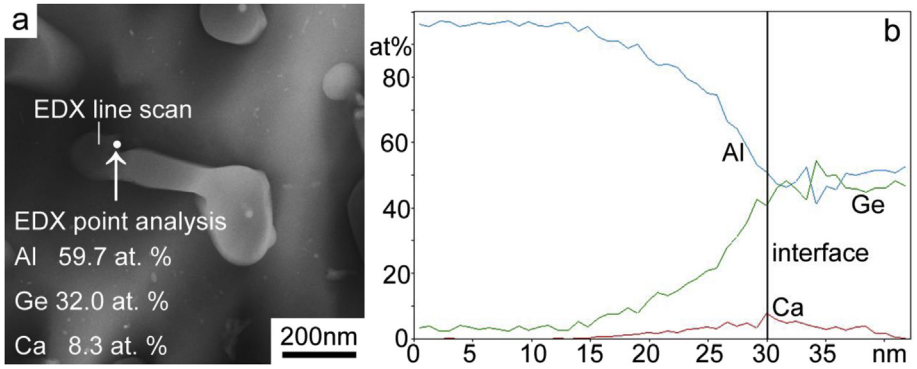

Fig. 5. (a) HAADF STEM image and (b) EDX line scan across the eutectic Al–Ge interface marked in (a) in Al–20Ge–0.2Ca alloy.

cylinder with a radius of 2 nm is presented in Fig. 12c. The Ca-enriched particle contains Al (32.02 ± 2.78 at%), Ge (58.28 ± 2.18 at%), Ca (5.98 ± 3.27 at%), and O (3.72 ± 3.13 at%).

4. Discussion

4.1. Eutectic Ge without additions of Y and Ca

The unmodified Al–20Ge alloy as shown in Fig. 1a and b is typically coarse and presents a eutectic structure containing almost lamellar Ge. The eutectic Ge lamellae do not have a sharp faceted morphology, which is in contrast to eutectic Si which typically forms sharp needles in two dimensions. Furthermore, the region of the eutectic Ge in Fig. 1b reveals the lamellar Ge plates almost perpendicular to each other, indicating that the growth of Ge appears along defined crystallographic directions, typically $<110>_{Ge}$ [1]. The observed lamellae morphology can be attributed to the strong anisotropy of Ge, the low interfacial energy between Ge and Al and the volume fraction of the minor phase which is close to 0.3 in the Al–20Ge alloy [18]. The lamellae eutectic Ge structure can be interpreted by the fact that it grows straight in advance with respect to the eutectic Al phase [1]. The lamellae structure can

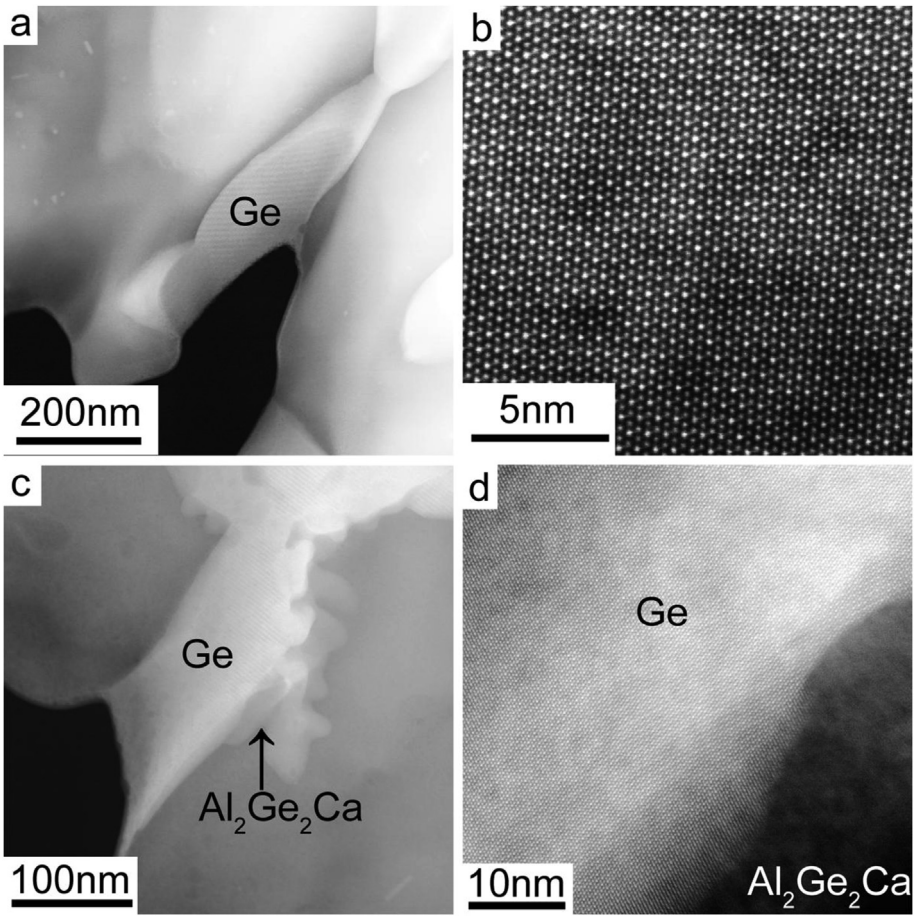

Fig. 6. HAADF STEM images of the Ge particle and the Al_2Ge_2Ca phase in Al–20Ge–0.2Ca alloy ($[011]_{Ge}$ zone axis orientation).

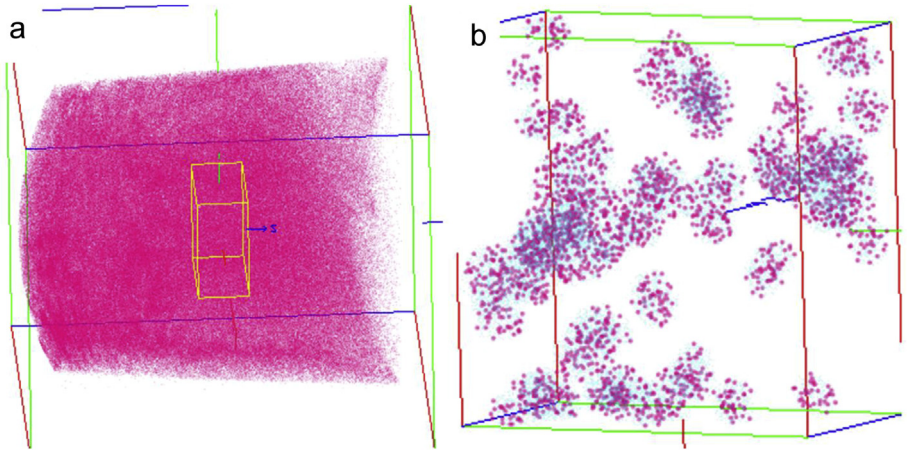

Fig. 7. (a) 3D reconstruction of Al (pink dots) atom positions within the eutectic Ge in Al–20Ge alloy. The investigated volume is 68 × 67 × 82 nm^3. For clarity the Ge atoms are omitted and only 20% of all measured Al atoms are displayed. (b) Sub-volume of 20 × 20 × 10 nm^3 (as marked in Fig. 7a) evaluated by cluster search. Al-rich clusters with the threshold of 10 at% of Al are visualized. (For interpretation of the references to colour in this figure legend, the reader is referred to the web version of this article.)

branch or change the growth direction by a large angle in response to the local conditions at the growth interface.

The eutectic Ge comprises a significantly higher concentration of Al, measured by APT to (5.43 ± 0.26) at%, than expected from the established binary Al–Ge phase diagram [1]. According to the binary Al–Ge phase diagram [1], the maximum solubility of Al in Ge is less than 2 at% at 400 °C. However, the eutectic Ge contains nanometer sized Al-enriched clusters with an average composition of ~14.14 ± 3.84 at%, which can explain the measured high amount of Al in eutectic Ge. Hence, the distribution of Al in the eutectic Ge phase is not homogeneous, which is in line with the case of eutectic Si. Al-rich precipitates in the size range from less than 10 nm to up to 40 nm are commonly observed in the eutectic Si during the solidification of Al–Si-based alloys [7–10,19,20]. Detailed

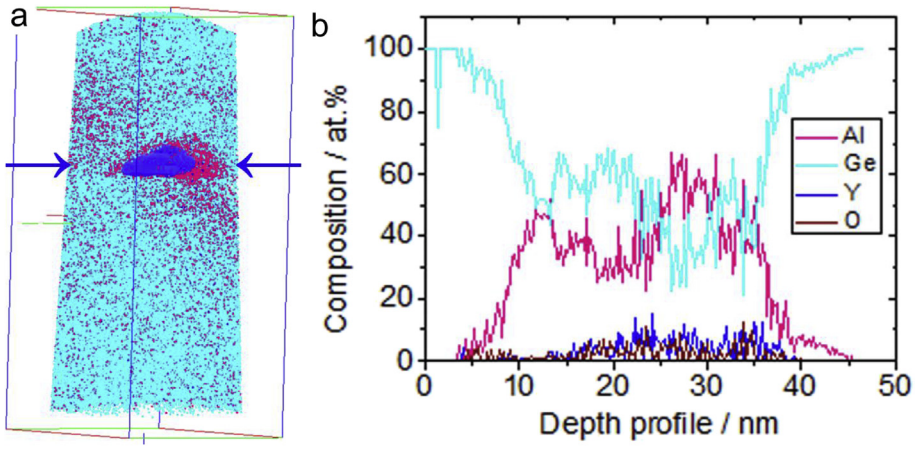

Fig. 8. (a) 3D reconstructions of the eutectic Ge phase in the Al–20Ge–0.2Y alloy. The investigated volume is 74 × 74 × 160 nm^3. For clarity, only15% of all measured Al (pink dots), 10% of all measured Y (blue dots) and only 1% of Ge (cyan) atom positions are plotted. High Y content is visualized by an iso-concentration surface (blue colour) at a threshold of 4 at % Y. (b) Corresponding depth profiles along the blue arrows as marked in (a). The concentration values were determined using slices with a thickness of 0.4 nm, a radius of 2 nm and a moving step of 0.2 nm. (For interpretation of the references to colour in this figure legend, the reader is referred to the web version of this article.)

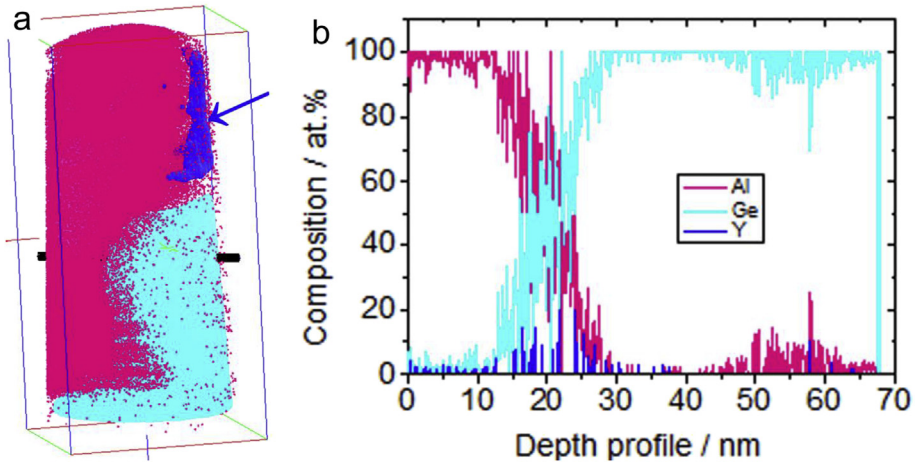

Fig. 9. (a) 3D reconstructions of eutectic Al (pink), represented by iso-concentration surface at a threshold of 75 at% Al and eutectic Ge (cyan) represented by iso-concentration surface at a threshold of 90 at% Ge in the Al–20Ge–0.2Y alloy. The investigated volume is 75 × 74 × 154 nm^3. An Y-rich region is visualized by an iso-concentration surface at a threshold of 20 at%, as marked by a blue arrow. (b) Concentration depth profiles across the interface between eutectic Al and eutectic Ge along the cylinder (indicated in (a)) with a radius of 1.5 nm. (For interpretation of the references to colour in this figure legend, the reader is referred to the web version of this article.)

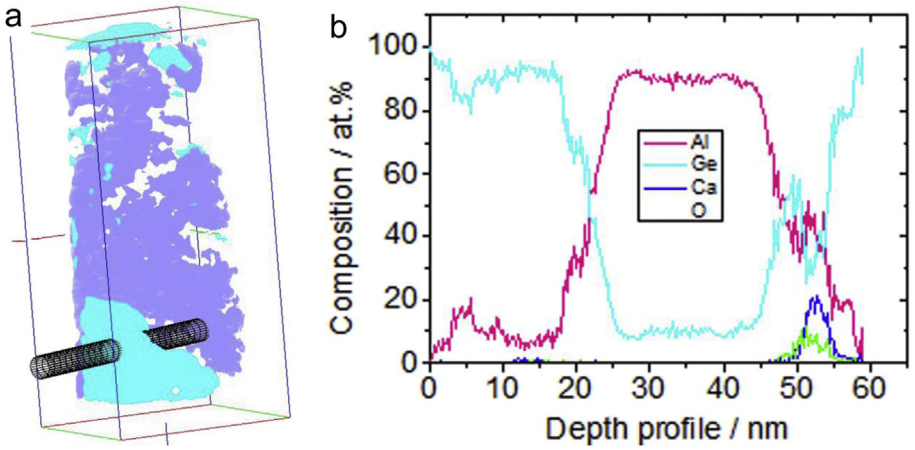

Fig. 10. (a) 3D reconstruction of eutectic Ge (cyan) visualized by an iso-concentration surface at a threshold of 85 at% Ge and Ca (purple) represented by an iso-concentration surface at a threshold of 8 at% Ca in the Al–20Ge–0.2Ca alloy. The investigated volume is 65 × 64 × 138 nm^3. For clarity, the eutectic Al phase has not been visualized. (b) Composition depth profiles along the cylinder with a radius of 4 nm oriented perpendicularly to the interface between eutectic Al and eutectic Ge, as shown in (a). (For interpretation of the references to colour in this figure legend, the reader is referred to the web version of this article.)

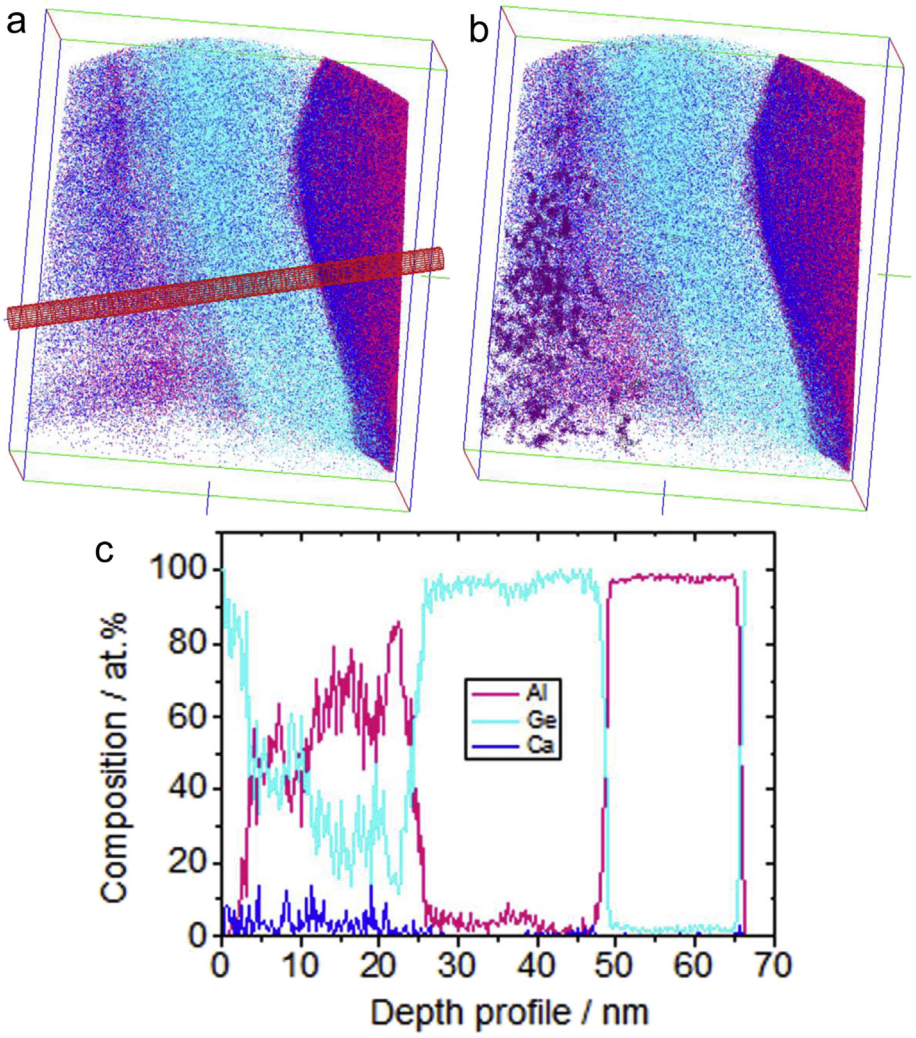

Fig. 11. (a) 3D reconstruction of the eutectic Al and Ge phases in the Al–20Ge–0.2Ca alloy. (Only 5% of all measured Al atoms, 2% of all measured Al atoms, and 50% of all measured Ca atoms are represented.). The investigated volume is $70 \times 69 \times 79$ nm^3. Ca-rich clusters (purple) with a threshold of 20 at% are visualized in (b). (c) Concentration depth profiles along a cylinder with a radius of 1 nm oriented perpendicularly to the interface between eutectic Al and eutectic Ge, as marked in (a). (For interpretation of the references to colour in this figure legend, the reader is referred to the web version of this article.)

investigations on atomic scale in Ref. [10] indicated Al segregations decorating defects on different length scale with compositions of up to 80–90 at% Al. Al-rich precipitates in the study published in Ref. [20] have been found to be associated with small amounts of oxygen or copper depending on the alloy composition. In the study published in Ref. [19] larger Al particle-void complexes were found. It was suggested that during Al precipitation the voids are created as a balance for the lower specific volume of Al with respect to the surrounding Si. The morphology and the size were found independent from the heat treatment.

The Al-clusters in the present study of eutectic Ge were not associated with lattice defects (dislocation or void formation) or metallic impurities. Their formation cannot be, therefore, compared with that in Al–Si alloys [7–10,19,20]. Most remarkable, the clusters are far smaller in the present study. The high amount of Al in eutectic Ge may further be explained by the fact that during solidification of Ge, diffusion has to occur in front of the liquid–solid interface, which may be influenced by trapping impurities like oxygen which was detected in small amounts in the present study in the Al-rich clusters. If the diffusion is incomplete, the solid may become supersaturated with Al.

4.2. Eutectic Ge in alloys with Y and Ca additions

Finding a reasonable correlation between the morphology of eutectic Ge, twin density, growth rate and distribution of Y and Ca additions in the Al–Ge eutectics is a big challenge. The eutectic Ge phase formed with additions of Y and Ca (Fig. 1c and e, respectively) is visible finer than that of the unmodified Al–20Ge alloy (Fig. 1a). Upon modification with Ca, eutectic Ge forms a spherical particle structure, at least as seen in 2D projections as shown in Fig. 1f. Spherical particles usually form when the interfacial energy is high and the phase tries to minimize the surface area [21]. However, as clarified by 3D imaging (not shown here) the morphology reveals to be not spherical but prolate. Clearly, the size and the morphology of the eutectic Ge is significantly affected by the Y and Ca additions. Presumably, the growth advance of Ge in modified alloy is lost according to [1]. Instead of fast growing of Ge as plates the morphological change of eutectic Ge is obtained. The proposed "poisoning" effect [6,22] on Ge plate growth mechanism which reduces its potential growth rate relative to the aluminium could be the mechanism for the effect of a modifying.

The low density of twins in eutectic Ge observed in TEM

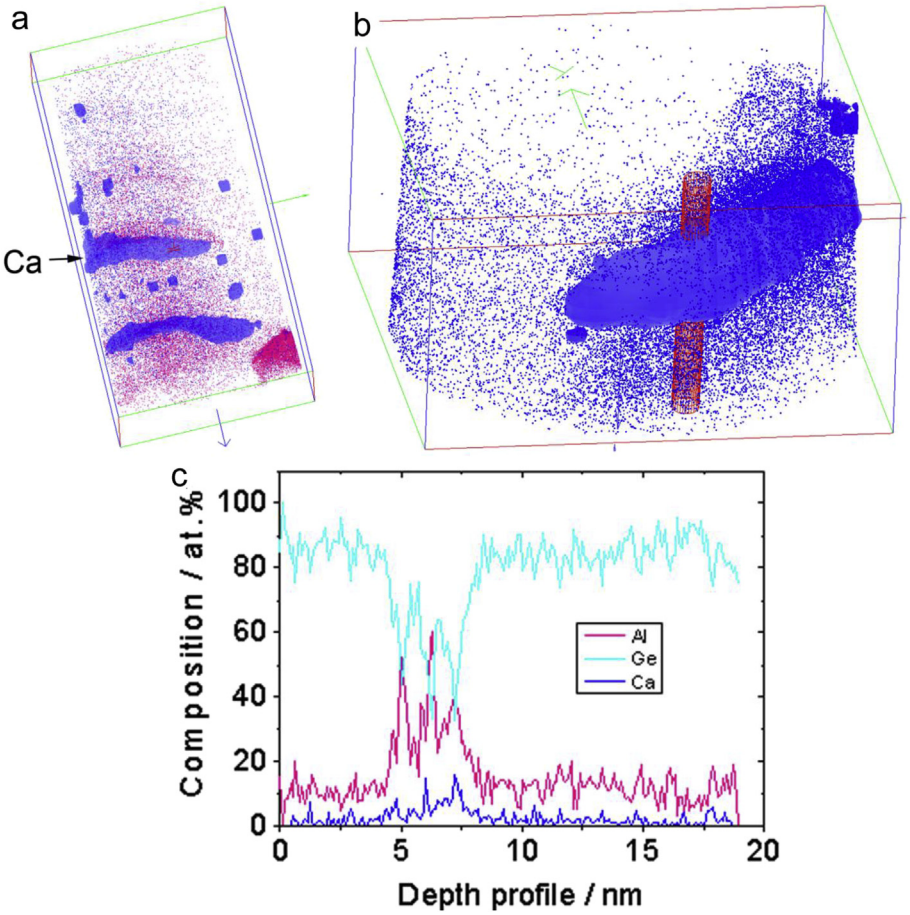

Fig. 12. (a) 3D reconstruction of the eutectic Ge in the Al–20Ge–0.2Ca alloy. (Only 50% of all measured Ca atom positions and 10% of all measured Al atoms are represented. Ge atoms have been omitted). The investigated volume is 73 × 75 × 142 nm^3. Ca-rich regions are emphasized by an iso-concentration surface at a threshold of 2.5 at% Ca. (b) A single Ca-rich region within the eutectic Ge selected from (a). The displayed volume is 63 × 71 × 37 nm^3. (c) Composition profiles across the Ca-rich cluster determined along a cylinder with a radius of 2 nm, as marked in (b).

investigations (see Fig. 2) is in contrast to the high density of twins obtained in eutectic Si of Al–Si alloys [9,10]. Furthermore, the density of twins was not significantly increased by additions of Y to the Al–Ge alloy (Figs. 3 and 4). Moreover, in the alloy with additions of Ca (Fig. 5) no twins were observed at all. However, a low twin density or even absence of twins was also observed in the pure binary Al–Si alloy, when it was quench solidified as reported in Ref. [3]. Since the cooling rate (200 °C/min) of the present alloys was relatively high, the fast quenching may be responsible for the low twin density observed in this study. The fact that Y was found to segregate together with Al on the nanometer scale across the twins shown in Fig. 4 indicates that such Al–Y co-segregations may promote the creation of new twins as demonstrated in Refs. [9,10] for eutectic Si. However, the density of the twins in Al–20Ge–0.2Y alloy is so low that they do not play a significant role in controlling the morphology of eutectic Ge. Since the observed parallel Ge twins (Fig. 2) are fully consistent with the TPRE mechanism, the TPRE growth mechanism may be also effective in the eutectic Ge of the as-cast Al–20Ge alloy. The importance of twinning for the growth mechanism was intensively studied in Al–Si alloys [3,23,24]. However, in a later study [24], no significant twin density was found in Si when modified by Ba and Ca or refined by Y and Yb. The low density or the absence of twins in the eutectic Ge of the Al–20Ge–0.2Y or Al–20Ge–0.2Ca alloys in the present study definitely cannot explain the modification of Ge by impurity induced twinning growth mechanism which is in accordance with results obtained previously [3,24].

The presence of Ca- or Y-rich segregations at the interface between eutectic Ge and eutectic Al as measured by TEM (Fig. 5) and by APT (Figs. 9b and 10b) definitely changes the local conditions at the migrating interface. We suppose that such segregations are also adsorbed at the re-entrant edges at the solid–liquid growth front of Ge and thereby prevent its further growth in the current direction by the TPRE mechanism. In consequence, the eutectic Ge crystal changes its growth to more energetically favoured directions.

The Al–Ca co-segregation shown in Figs. 11c and 12c inside the eutectic Ge does obviously not promote twinning, because no twins were observed by TEM. However, such co-segregations may prevent its further growth in the current direction and thereby change the microstructure of eutectic Ge. Such co-segregations may play the key role in modifying Al–Ge alloys. They contribute to the morphological change of the eutectic Ge and not to the twinning as has been predicted for Al–Si alloy in Ref. [23].

In the case of Y additions, an interconnected structure of the eutectic Ge was observed in 2D projection, as shown in Fig. 1d. However, Fig. 1c and d clearly show that there are two different morphologies of the eutectic Ge phase, as marked by “1” and “2” in Fig. 1c,d. In the region “1”, there is a complex structure with highly curved interfaces and a vermicular shape, rather than an interconnected plate-shaped morphology. In the region “2”, a continuous region eutectic Ge phase is seen, in which a rod-like eutectic Al is embedded. Clearly, there is a different effect of Y additions and

Ca additions on the growth of eutectic Ge, which can be attributed to the different spatial distribution of Ca and Y. While Ca is mainly distributed within the eutectic Ge and at the interface between eutectic Ge and eutectic Al, Y is mostly distributed within the eutectic and the primary Al, forming AlY clusters. The presence of Y within the eutectic Al and primary Al may also affect the growth of eutectic Al and finally may only indirectly change the growth of eutectic Ge.

5. Conclusions

A multi-scale microstructure characterization, including SEM, HRTEM, HAADF-STEM and APT, has been used to investigate the effects of 0.2Y and 0.2Ca on the eutectic Ge in Al–20 Ge alloys. The main conclusions can be drawn:

1. Within the eutectic Ge of as-cast Al–20Ge alloy, parallel Ge twins were observed, indicating that the TPRE growth mechanisms may be effective for the growth of the eutectic Ge.
2. The high amount of Al in eutectic Ge is suggested due to the incomplete Al diffusion in front of the liquid–solid interface during solidification. Hence, the eutectic Ge becomes supersaturated with Al and this can explain the presence of small Al-rich clusters within the eutectic Ge of the as-cast Al–20Ge alloy.
3. Addition of 0.2 wt% Ca or 0.2 wt% Y to the binary Al–Ge alloy has a significant impact on the growth and morphology of the eutectic Ge phase.
4. Within the eutectic Ge, the distribution of Ca was observed by APT to be heterogeneous in form of Ca-enriched clusters of very small size. In addition, few large Ca-enriched particles were observed by APT, which may be due to the solute entrainment during the growth of eutectic Ge. In contrast, only a trace Y, but, no significant Y-rich clusters were detected by APT. By HAADF-STEM, an enrichment of Y (about 5 at%) along the Ge twins was detected, which is believed to promote the impurity induced twinning. However, the density of twins in alloy with Y addition is very low.
5. At the interface between eutectic Al and eutectic Ge, large Ca-rich particles, most likely of the Al_2Ge_2Ca phase, were observed. In contrast, no Y-rich phase was observed at the interface between eutectic Al and eutectic Ge. Instead, most Y is located within the eutectic Al, forming AlY clusters there.
6. The low density of twins or the absence of twins obtained in eutectic Ge with Y and Ca additions strongly indicates that the IIT mechanism is not relevant for the modification of eutectic Ge.
7. As the Al–Ca co-segregations inside the eutectic Ge do not promote twinning, they inhibit the growth of eutectic Ge in the current direction and thereby induced the morphological change from plate to prolate.

Acknowledgements

J.H. Li acknowledges the access to the TEM facility at the Erich Schmidt Institute of Materials Science of the Austrian Academy of Sciences and the financial support from the Major International (Regional) Joint Research Project (No. 51420105005) from China. Mrs. Christiane Förster is acknowledged for sample preparation for SEM investigations. The HAADF-STEM analysis at the Graz Center for Electron Microscopy has received funding from the FFG under project no. 839083(COIN OPTIMATSTRUCT) and European Union within the 7th Framework Program [FP7/2007–2013] under grant agreement no. 312483 (ESTEEM2).

References

[1] A. Hellawell, The growth and structure of eutectics with silicon and germanium, Prog. Mater. Sci. 15 (1970) 3–78.
[2] A. Pacz, Alloy. U.S Patent No. 1387900; 1921.
[3] S.Z. Lu, A. Hellawell, The mechanism of silicon modification in aluminium – silicon alloys: impurity induced twinning, Metall. Trans. A 18 (1987) 1721–1733.
[4] R.S. Wanger, On the growth of germanium dendrites, Acta Metall. 8 (1960) 57–60.
[5] R.D. Hamilton, R.G. Seidensticker, Propagation mechanism of germanium dendrites, J. Appl. Phys. 31 (1960) 1165.
[6] M.G. Day, A. Hellawell, The microstructure and crystallography of aluminium–silicon eutectic alloys, Proc. R. Soc. Lond. A 305 (1968) 473–491.
[7] J.H. Li, M. Zarif, M. Albu, B. McKay, F. Hofer, P. Schumacher, Nucleation kinetic of eutectic Si in entrained Al–5Si alloys, Acta Mater. 72 (2014) 80–98.
[8] J.H. Li, M. Albu, F. Hofer, P. Schumacher, Solute adsorption and entrapment during eutectic Si growth in A–Si-based alloys, Acta Mater. 83 (2015) 187–202.
[9] M. Timpel, N. Wanderka, R. Schlesiger, T. Yamamoto, N. Lazarev, D. Isheim, G. Schmitz, S. Matsumura, J. Banhart, The role of strontium in modifying aluminium–silicon alloys, Acta Mater. 60 (2012) 3920–3928.
[10] J. Barrirero, M. Engstler, N. Ghafoor, N. de Jonge, M. Oden, F. Mücklich, Comparison of segregation formed in unmodified and Sr-modified Al–Si alloys studied by atom probe tomography and transmission electron microscopy, J. Alloy Compd. 611 (2014) 410–421.
[11] H. Song, A. Hellawell, Solidification in the system Al–Ge–Si: the phase diagram, coring patterns, eutectic growth, and modification, Metall. Trans. A 21 (1990) 733–740.
[12] L. Reimer, Scanning Electron Microscopy: Physics of Image Formation and Microanalysis, Springer, Berlin, 1998.
[13] J.I. Goldstein, D.B. Williams, G. Cliff, Quantification of energy, in: D.C. Joy, A.D. Romig, J.L. Goldstein (Eds.), Dispersive Spectra in Principles of Analytical Electron Microscopy, Plenum Press, New York, 1986, pp. 155–217.
[14] R. Schlesiger, C. Oberdorfer, R. Würz, G. Greiwe, P. Stender, M. Artmeier, P. Pelka, F. Spaleck, G. Schmitz, Design of a laser-assisted tomographic atom probe at Münster University, Rev. Sci. Instrum. 81 (2010) 043703.
[15] J.W. Edington, Practical Electron Microscopy in Material Science, Techbooks, Fairfax, VA, 1991.
[16] X. Sauvage, G. Dacosta, R.Z. Valiev, Ultra grained materials III, in: Y.T. Zhu, T.G. Langdon, R.Z. Valiev, S.L. Semiatin, D.H. Shin, T.C. Lowe (Eds.), 3D Atom Probe Investigation of Cementite Dissolution in a Perlitic Steel Processed by High Pressure Torsion, TMS (The Minaerals, Metals & Materials Society), Warrendale, PA, 2004, pp. 31–36.
[17] H.Z. Wang, Y.Z. Zhan, M.J. Pang, Y. Du, Properties of hexagonal Al_2Ge_2RE (RE = Y, La, Ce, Nd, Eu, Gd, Tb, Yb, and Lu): a first-principles study, Solid State Commun. 151 (2011) 1814–1819.
[18] W. Kurz, D.J. Fischer, Fundamentals of Solidification, Trans Tech Publications, 1998.
[19] Z.H. Jia, L. Arnberg, S.J. Andersen, J.C. Walmsley, On nanoscale Al precipitates forming in eutectic Si particles in Al–Si–Mg cast alloys, Scr. Mater. 61 (2009) 500–503.
[20] K. Nogita, H. Yasuda, M. Yoshiya, S.D. McDonald, K. Uesugi, A. Takeuchi, Y. Suzuki, The role of trace element segregation in the eutectic modification in hypoeutectic Al–Si alloys, J. Alloy Compd. 489 (2010) 415–420.
[21] W.T. Donlon, Precipitation of aluminium in silicon phase contained W319 and 356 aluminium alloys, Metall. Mater. Trans. 34A (2003) 523–529.
[22] K.F. Kobayashi, L.M. Hogan, The crystal growth of silicon in Al–Si alloys, J. Mater. Sci. 20 (1985) 1961–1975.
[23] M. Shamsuzzoha, L.M. Hogan, The crystal morphology of fibrous silicon in strontium modified Al–Si eutectic, Philos. Magn. A 54 (1986) 459–477.
[24] K. Nogita, J. Drennan, A.K. Dahle, Evaluation of twinning in hypo-eutectic Al–Si alloys, Mater. Trans. 44 (2003) 625–628.